INTERNATIONAL JOURNAL OF
NUMERICAL ANALYSIS AND MODELING
Volume 17, Number 5, Pages 746–765



# A CORRECTED NEAREST NEIGHBOR TRANSPOTATION METHOD OF AERODYNAMIC FORCE FOR FLUID-STRUCTURE INTERACTIONS

YUNZHEN LIU, ZHIQIANG WAN, QIA LI, AND QINGHUI ZHANG*

**Abstract.** Aeroelastic analysis of the aircraft is a typical fluid-structure interaction problem. It is influenced by interactions between aerodynamic forces and deformations of elastic structures. The aerodynamic field and structural deformation are modeled by different physical equations, and the associated computational meshes do not match each other. Therefore, passing data from a mesh to the other one in a physically reasonable way is a challenging task. Current aerodynamic force transportation methods, such as virtual work conserved method (VWC), area weighted shape function method (AWSF), proximity minimum strain energy method (PMSE), and inverse distance weighted method (IDW), either destroy physical conservations or cause unreasonable distributions of structural forces. In this paper we propose a corrected nearest neighbor transportation method (CNNT) of aerodynamic force for the fluid-structure coupling analysis. The force transportation process is divided into two phases. First, the aerodynamic forces are allocated to the structural nodes initially using the conventional methods or, e.g., AWSF, IDW. Then, the initially allocated structural forces are corrected by solving an optimization problem with the physical conservations as its optimization target. The optimization problem is solved by a barrier interior point method efficiently.A sport airplane model is employed to verify effectiveness of CNNT. Comparisons with the VWC, AWSF, PMSE, IDW are also made. The numerical experiments show that the CNNT maintains the force, moment, and virtual work conservations, and exhibitsreasonable distributions of structural forces, indeed.

**Key words.** Aerodynamic force transportation, fluid-structure interaction, nearest neighbor method, and corrected algorithm.

## 1. Introduction

Aeroelastic analysis of the aircraft is a typical fluid-structure interaction problem. It is influenced by the interactions between deformations of elastic structures caused by fluid flows and aerodynamic forces decided by structure frameworks. Loose couplings adopt a three-field formulation, the aerodynamic model, structural model, and the coupling process. Such schemes have advantages that each component of coupling problems can be handled as an isolated identity. The aerodynamic field can be modeled by Navier-Stokes or Eular equations that can be solved for example by finite volume methods or panel methods, while the structural deformation is modeled by elasticity theory that can be solved in general by finite elements methods. These two models describe the interfaces of the aircraft using different resolutions so that the meshes they use don't match each other. Therefore, the challenging task is to pass data from a mesh to the other one in a physically reasonable way. Specifically, aerodynamic forces need to be transferred from fluid to structure, while structure displacements need to be interpolated form structure back to fluid. In the process of data exchange, five criteria should be satisfied [1, 2]: (1) global conservations of forces and moments; (2) accurate displacement interpolations; (3)

Received by the editors February 1, 2020 and, in revised form, May 14, 2020.
2000 *Mathematics Subject Classification.* 74F10,65K10,65N30,65D05.
*Corresponding author. Email: zhangqh6@mail.sysu.edu.cn.

global conservations of virtual works; (4) consistency of local loads; (5) stability and efficiency.

In aspect of the displacement interpolations, the interpolation accuracy rather than the conservations of physical quantities is a main focus. Therefore, various interpolation methods with high accuracies can be taken as choices. In general, the displacement interpolation methods are divided into local interpolation methods and global interpolation methods [3].The local interpolation methods, such as nodal projection method [4, 5],weighted residual method [6] and constant volume method [7], produces interpolation matrices that are sparse and can be solved quickly. However, it requires additional mesh information and searching process, which will increase the computational complexity. The global displacement interpolation methods are easily implemented, but yield full interpolation matrices, such as infinite panel spline (IPS) method [8], finite plate spline (FPS) [9], thin plate spline (TPS) [10], multi-quadric spline (MQ) [11], and Shepard method [12]. Compared with the methods above, radial basis function (RBF) spline methods [13, 14] perform the interpolation on various sub-regions of an aircraft, and show advantages in dealing with a large number of scatter data. The RBF spline interpolation methods have been widely used in fluid-solid coupling analysis in [15–18]. It was investigated in [19, 20] that the TPS and MQ are superior to the other RBF with the most robust, easily implemented, and accurate properties. In this paper, we adopt the TPS based radial basis function to fulfill the displacement interpolation.

On the other hand, the aerodynamic forces need to be transferred from fluid nodes to structure nodes. This process is significantly different from the displacement interpolation because the conservations of total forces, moments, virtual works, and reasonable distributions of forces are required. A generally used method for the force transportation is a so-called virtual work conserved method (VWC), which is embedded into conventional FE softwares, like the MSC-Nastran. The VWC derives the transportation formulation based on the law of virtual work conservation, and the associated transportation matrix is just the transpose of the displacement interpolation matrix [21]. The load is also globally conserved by the VWC. However, it usually causes unreasonable local force distributions in a sense that the transported forces may be opposite to the associated aerodynamic forces on some local structural nodes. Various local methods are also commonly used for the force transportation, and the main idea of these methods is to distribute an aerodynamic force to the structural nodes in its nearest neighborhood. For instance, an area weighted shape function method (AWSF) [22] finds the nearest three structural nodes of a fluid node to construct a triangle and distribute the aerodynamic force according to the area weights, a proximity minimum strain energy method (PMSE) [23]chooses the several nearest structural nodes to allocate the aerodynamic force by assuming the load conservation laws and minimizing a strain energy, an inverse distance weighted method (IDW) [12]also chooses the nearest structural nodes, but allocates the force using the inverses of Euclidean distances between structure node and fluid nodes as weights. Even though the load distributions of these local methods are relatively reasonable, compared with the VWC, the physical conservations are destroyed, such as the virtual works are not maintained by all three methods, while the moments are not preserved by the AWSF and IDW. Moreover, in the AWSF some structure nodes may get no force, and in the PMSE, local force deviations may appear in areas with high curvatures or irregular distributions of structure nodes. To our best knowledge, an aerodynamic

force transportation method with the physical conservations and reasonable force distributions has not been reported in the literature.

In this paper we propose a corrected nearest neighbor transportation method (CNNT) of aerodynamic forces for the fluid-structure coupling analysis. The force transportation process is divided into two phases. First, the aerodynamic forces are allocated to the structural nodes initially. This can be fulfilled using the above-mentioned local methods or their combinations, e.g., AWSF, IDW, where the IDW is relatively preferable because of its excellent local performance and easy implementation. Second, the initially allocated structural forces are corrected by solving an optimization problem with the physical conservations as its optimization target. Specifically, the force, moment and virtual work deviations between fluid and structure are summed together as the objective function, and small percentage deviations of the initial forces serve as the upper and lower bounds of constrains. The optimization problem is solved by a barrier interior point method efficiently. The proposed CNNT is used on a sport airplane to verify its effectiveness. The numerical experiments show that the CNNT maintains the force, moment, and virtual work conservations, and exhibits reasonable distributions of structural forces indeed. The results of VWC, AWSF, PMSE, IDW are also presented for comparison.

The rest of the paper is organized as follows.The model problem and displacement interpolation are described in Section 2.Four conventional aerodynamic force transportation methods are introduced in Section 3.In Section 4, the CNNT method is proposed,and corresponding numerical schemes are presented. In section 5, the results of different aerodynamic force transportation methods are compared in global and local performance using a sport airplane model. Conclusions are given in the last section.

## 2. Model problem and preliminaries

We denote the coefficients of a point in $\mathbf{R}^3$ by $P(x, y, z)$.The basis of polynomials of degree $k$ is denoted by $\{s_l(P)\}_{l=1}^m$. For $k = 1$, i.e., the linear polynomials, $m = 4$ and $\{s_l(P)\}_{l=1}^4 = \{1, x, y, z\}$.

Let X be a model of aircraft that is discretized by a structural mesh G with coefficients of nodes, $P_{Gi} = (x_{Gi}, y_{Gi}, z_{Gi}), i = 1, 2, ..., n_G$, $n_G$ is the number of nodes. The aerodynamic (or fluid) mesh K is shown in FIGURE 1 UP. The nodes of K that represent the center points of fluid elements are denoted by $Q_{Ki} = (x_{Ki}, y_{Ki}, z_{Ki}), i = 1, 2, ..., n_K$, $n_K$ is the number of nodes. The meshes G and K are created from different models for structural and fluid analyses, respectively. According to different requirements of resolutions and computational models, G and K do not match inevitably; see FIGURE 1 DOWN for an illustration of non-matching meshes. Therefore, passing data from one mesh to the other one is a key to success of the fluid-structure analysis. This involves two aspects: transferring aerodynamic forces from K to G to calculate displacements of structure nodes (hollow circles) and interpolating structure displacements (or deformations) from G to K to fluid nodes to recalculate the aerodynamic forces. Below, we use $\mathbf{u}_G = \{u_{Gi}\}_{i=1}^{n_G}$, $\mathbf{F}_G = \{F_{Gi}\}_{i=1}^{n_G}$ and $\mathbf{u}_K = \{u_{Ki}\}_{i=1}^{n_K}$,$\mathbf{F}_K = \{F_{Ki}\}_{i=1}^{n_K}$ to denote displacements and forces on fluid and structure, respectively.

As discussed in Introduction, in the stage of displacement interpolations, the accuracy rather than the conservations of physical quantities is a main concern.The (RBF) spline method [13, 14] has been widely used in fluid-solid coupling analysis in [15–18]. It performs the interpolation on various sub-regions of an aircraft and turns to be robust, easily implemented, and accurate, see [19, 20] for instance.

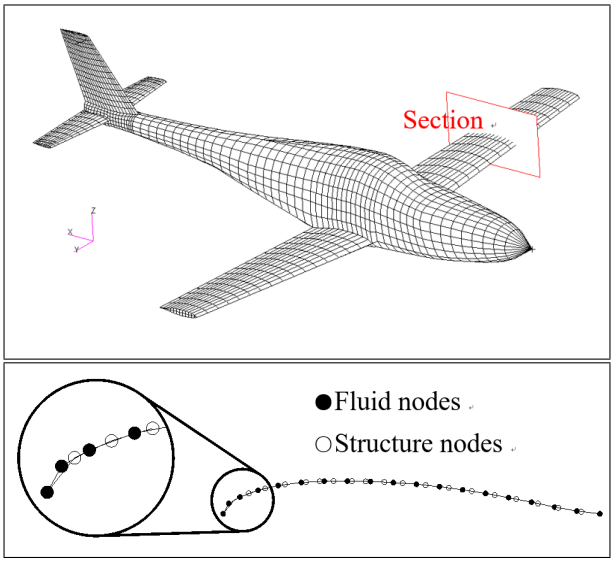


FIGURE 1. UP: An aircraft with a fluid mesh; Down: Non-matching meshes between fluid and structure in a section of aircraft wing.

In the RBF interpolation, the displacement $u(P)$ of any point $P(x, y, z)$ on the fluid and structure interface is approximated in a general form of

$$u(P) = \sum_{j=1}^{n_G} R_j(P)a_j + \sum_{l=1}^{m} s_l(P)b_l, \tag{1}$$

where $s_l, l = 1, 2, ..., m$, are the base functions of polynomials, $R_j(P)$ is the $j$th radial basis function:

$$R_j(P) = \varphi(\|P - P_{Gj}\|), \|P - P_{Gj}\| = \sqrt{(x - x_{Gj})^2 + (y - y_{Gj})^2 + (z - z_{Gj})^2}, \tag{2}$$

and $\varphi(r) := r^2 \ln(r^2)$ is the thin-plate spline (TPS) radial basis function.The coefficients $a_j$ and $b_l$ are determined by the known displacement of structure nodes.

Assuming $\mathbf{u}_G$ are the known displacements of $n_G$ structure nodes, then the matrix form of (1) is

$$\mathbf{u_G} = \mathbf{R_{GG}a_G} + \mathbf{P_{Gm}b_m}. \tag{3}$$

where $\mathbf{a_G}$ and $\mathbf{b_m}$ are the associated vector forms of coefficients.

Radial basis function matrix $\mathbf{R_{GG}}$ and the polynomial matrix $\mathbf{P_{Gm}}$ are

$$\mathbf{R_{GG}} = [R_j(P_{Gi})]_{i,j=1,...,n_G}, \text{and } \mathbf{P_{Gm}} = [s_l(P_{Gi})]_{i=1,...,n_G, l=1,...,m}.$$

In this paper,we consider $m = 4$,then $\mathbf{P_{Gm}}$ is simplified as

$$\mathbf{P_{Gm}} = [1 \ x_{Gi} \ y_{Gi} \ z_{Gi}]_{i=1,...,n_G}.$$

By adding the additional constraint condition,

$$\sum_{i=1}^{n_G} s_l(P_{Gi})a_l = 0, \ l = 1, 2, ..., m, \tag{4}$$

the discrete structure displacement(1) and the constraint condition(4) can be written as follows:

$$\begin{bmatrix} \mathbf{u_G} \\ \mathbf{0_m} \end{bmatrix} = \begin{bmatrix} \mathbf{R_{GG}} & \mathbf{P_{Gm}} \\ \mathbf{P_{Gm}^T} & \mathbf{0_{mm}} \end{bmatrix} \begin{bmatrix} \mathbf{a_G} \\ \mathbf{b_m} \end{bmatrix}. \tag{5}$$

Once the coefficients of $\mathbf{a_G}$ and $\mathbf{b_m}$ are solved in (5), we derive the displacement of any fluid nodes by

$$\mathbf{u_K} = \begin{bmatrix} \mathbf{R_{KG}} & \mathbf{P_{Km}} \end{bmatrix} \begin{bmatrix} \mathbf{a_G} \\ \mathbf{b_m} \end{bmatrix}, \tag{6}$$

where

$$\mathbf{R_{KG}} = [R_j(Q_{Ki})]_{i=1,\ldots,n_K, j=1,\ldots,n_G}, \text{and } \mathbf{P_{Km}} = [s_l(Q_{Ki})]_{i=1,\ldots,n_K, l=1,\ldots,m}.$$

## 3. Conventional aerodynamic force transportation methods

In this section, we introduce several conventional aerodynamic force transportation methods and analyze their features in aspects of conservations of physical quantities and distributions of forces. They are virtual work conserved method (VWC), area weighted shape function method (AWSF),minimum proximity strain energy method (MPSE) and inverse distance weighted method (IDW).

### 3.1. Virtual work conserved method.

According to (5) and (6), the relationship between fluid displacement $\mathbf{u_K}$ and structure displacement $\mathbf{u_G}$ is given by:

$$\mathbf{u_K} = \begin{bmatrix} \mathbf{R_{KG}} & \mathbf{P_{Km}} \end{bmatrix} \begin{bmatrix} \mathbf{R_{GG}} & \mathbf{P_{Gm}} \\ \mathbf{P_{Gm}^T} & \mathbf{0_{mm}} \end{bmatrix}^{-1} \begin{bmatrix} \mathbf{u_G} \\ \mathbf{0_m} \end{bmatrix}. \tag{7}$$

Then the virtual displacement would be

$$\delta\mathbf{u_K} = \begin{bmatrix} \mathbf{R_{KG}} & \mathbf{P_{Km}} \end{bmatrix} \begin{bmatrix} \mathbf{R_{GG}} & \mathbf{P_{Gm}} \\ \mathbf{P_{Gm}^T} & \mathbf{0_{mm}} \end{bmatrix}^{-1} \begin{bmatrix} \delta\mathbf{u_G} \\ \mathbf{0_m} \end{bmatrix}. \tag{8}$$

On the other hand,the virtual works of the fluid $\delta W_K$ and the structure $\delta W_G$ acting on the interface can be written respectively as

$$\delta W_K = \mathbf{F}_K^T \delta\mathbf{u}_K, \delta W_G = \mathbf{F}_G^T \delta\mathbf{u}_G. \tag{9}$$

Employing the conservation of the virtual works, i.e., $\delta W_K = \delta W_G$, we have

$$\mathbf{F}_K^T \delta\mathbf{u}_K = \mathbf{F}_G^T \delta\mathbf{u}_G = \begin{bmatrix} \mathbf{F_G^T} & \mathbf{0} \end{bmatrix} \begin{bmatrix} \delta\mathbf{u_G} \\ \mathbf{0_m} \end{bmatrix}. \tag{10}$$

Then substituting (8) into (10), we derive the transported forces $\mathbf{F}_G$ as follows:

$$\begin{bmatrix} \mathbf{F}_G \\ \mathbf{0_m} \end{bmatrix} = \left( \begin{bmatrix} \mathbf{R_{KG}} & \mathbf{P_{Km}} \end{bmatrix} \begin{bmatrix} \mathbf{R_{GG}} & \mathbf{P_{Gm}} \\ \mathbf{P_{Gm}^T} & \mathbf{0_{mm}} \end{bmatrix}^{-1} \right)^T \mathbf{F}_K. \tag{11}$$

This method is referred to as virtual work conserved method (VWC), which guarantees the equality of virtual works according to (10). It is a method embedded into conventional FE softwares, like the MSC-Nastran. The equation (11) is equivalent to

$$\begin{bmatrix} \mathbf{F}_G \\ \mathbf{0_m} \end{bmatrix} = \begin{bmatrix} \mathbf{R_{GG}} & \mathbf{P_{Gm}} \\ \mathbf{P_{Gm}^T} & \mathbf{0_{mm}} \end{bmatrix}^{-1} \begin{bmatrix} \mathbf{R_{KG}} & \mathbf{P_{Km}} \end{bmatrix}^T \mathbf{F}_K \Leftrightarrow \begin{bmatrix} \mathbf{R_{GG}} & \mathbf{P_{Gm}} \\ \mathbf{P_{Gm}^T} & \mathbf{0_{mm}} \end{bmatrix} \begin{bmatrix} \mathbf{F}_G \\ \mathbf{0_m} \end{bmatrix} = \begin{bmatrix} \mathbf{R_{KG}^T} \\ \mathbf{P_{Km}^T} \end{bmatrix} \mathbf{F}_K. \tag{12}$$

Focusing on the polynomial part of equation above gives

$$\mathbf{P}_{\mathbf{Gm}}^{\mathbf{T}}\mathbf{F}_{\mathbf{G}} = \mathbf{P}_{\mathbf{Km}}^{\mathbf{T}}\mathbf{F}_{\mathbf{K}}, \tag{13}$$

which implies the conservations of force and moment (see the equation(4) ).

The VWC keeps the conservations well. However, the equation (10) is a strong constraint, which could cause opposing structural forces on some local regions.

### 3.2. Area weighted shape function method.

Generally speaking, the initial result of fluid analysis is the pressure on fluid grid in CFD method. As the consistency of input and output between fluid analysis and structure analysis is required, it is improper to directly use the pressure to imply the conversions. Therefore, a relatively easy way is to convert integrated aerodynamic node forces to the structure model [24].In the area weighted shape function method (AWSF), each aerodynamic force on fluid node is transferred to three nearest structure nodes that form a suitable triangle and assigned according to the area weights.

First, for any fluid node $K$, we find the suitable triangle that consists of structure nodes and contains $K$ as an interior point. To keep the local consistency of load distribution, the closest triangle should be obtained, as the triangle $\Delta 234$ shown in FIGURE 2.

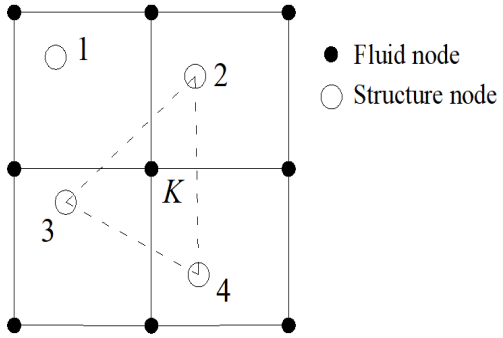


FIGURE 2. Fluid node and the relative structure nodes in triangle.

Denote the node $K$ and the three structure nodes in the triangle by $(x, y), (x_2, y_2)$, $(x_3, y_3), (x_4, y_4)$, respectively in two dimension, as shown in FIGURE 3.Then the areas of $S_2, S_3, S_4$ in FIGURE 3 can be calculated as follows:

$$S_2 = \frac{1}{2}\begin{vmatrix} x_3 & y_3 & 1 \\ x_4 & y_4 & 1 \\ x & y & 1 \end{vmatrix}, S_3 = \frac{1}{2}\begin{vmatrix} x_4 & y_4 & 1 \\ x_2 & y_2 & 1 \\ x & y & 1 \end{vmatrix}, S_4 = \frac{1}{2}\begin{vmatrix} x_2 & y_2 & 1 \\ x_3 & y_3 & 1 \\ x & y & 1 \end{vmatrix}.$$

The second step is to allocate the aerodynamic force $\mathbf{F}_K$ at the node $K$ to three nodes of $\Delta 234$ to derive the associated structural forces $\mathbf{F}_i$,$i$=2,3,4. Below in this section, we always use $F_K$ and $F_i$ to denote each component of $x, y, z$ components of $\mathbf{F}_K$ and $\mathbf{F}_i$, respectively. The structural forces at the three nodes of $\Delta 234$ are obtained as follows:

$$F_i = F_K \cdot S_i / \sum_{i=2}^{4} S_i, i = 2, 3, 4. \tag{14}$$

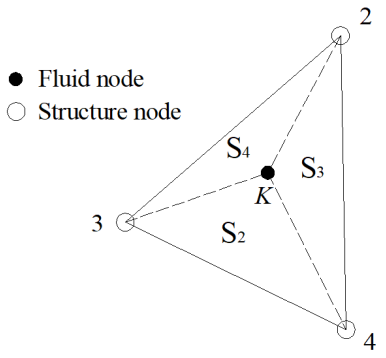


FIGURE 3. Area weight within the triangle.

According to this approach, the moment conservation can be easily verified by (15)

$$\begin{aligned} M_S &= \sum_{i=2}^{4} F_i|\vec{K}i| = \sum_{i=2}^{4} S_i|\vec{K}i|F_K/\sum_{i=2}^{4} S_i \\ &= \frac{1}{2}[(\vec{K}3\times\vec{K}4)\times\vec{K}2+(\vec{K}4\times\vec{K}2)\times\vec{K}3+(\vec{K}2\times\vec{K}3)\times\vec{K}4]F_K/\sum_{i=2}^{4} S_i \\ &= 0\cdot F_K/\sum_{i=2}^{4} S_i = 0 = M_K, \end{aligned}$$

where $M_S$ is the total moment caused by the forces on three structure nodes, $M_K$ is the moment caused by the aerodynamic force; here, the fluid node $K$ serves as the moment reference point.

Therefore, the AWSF can obey the law of force and moment conservations and local consistency of load distribution in two dimension. In three dimension, however, the fluid node is generally outside the plane of the triangle, which cause errors in the moments.

### 3.3. Proximity minimum strain energy method.

The proximity minimum strain energy method (PMSE) assumes that there is a virtual beam element between $n$ nearest local structure nodes and the fluid node $K$ as shown in FIGURE 4. As the fluid node fixed and the structure node allocated with force $F_i$, the strain energy of each beam is

$$U_i = \frac{1}{6EJ}F_i^2 l_i^3,$$

where $EJ$ is the bending stiffness of virtual beam,$l_i$ is the Euclidean distance between the $i$th structure node and the fluid node $K$.Then the total strain energy in the proximity is:

$$U = \sum_{i=1}^{n} U_i.$$

The forces distributed to the structure nodes are required to minimize the strain energy of system and satisfy the force conservation conditions. Assume the coefficients of structure nodes and fluid node are $(x_{Gi}, y_{Gi}, z_{Gi})$ and $(x_K, y_K, z_K)$,

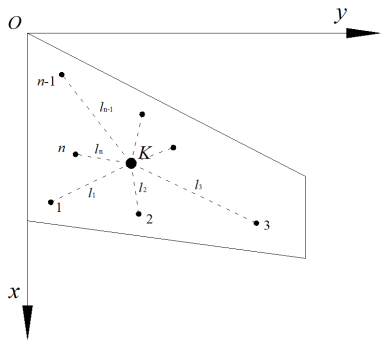


FIGURE 4. Virtual beams between the fluid node and the structure nodes.

respectively, and the direction of the force is constant before and after the transportation, then there are

$$\sum_{i=1}^{n} F_i = F_K; \sum_{i=1}^{n} F_i x_{Gi} = F_K x_K; \sum_{i=1}^{n} F_i y_{Gi} = F_K y_K; \sum_{i=1}^{n} F_i z_{Gi} = F_K z_K. \tag{16}$$

In order to get a dual problem of the above problem, the following Lagrange functionis introduced:

$$L(\lambda, \lambda_x, \lambda_y, \lambda_z) = \sum_{i=1}^{n} (\frac{1}{6EJ} F_i^2 l_i^3 - \lambda F_i - \lambda_x F_i \bar{x}_i - \lambda_y F_i \bar{y}_i - \lambda_z F_i \bar{z}_i),$$

where

$$(\bar{x}_i, \bar{y}_i, \bar{z}_i) = (x_{Gi}, y_{Gi}, z_{Gi}) - (x_K, y_K, z_K), l_i = \sqrt{\bar{x}_i^2 + \bar{y}_i^2 + \bar{z}_i^2}.$$

Considering the extreme conditions of the Lagrange function $\partial L(\lambda, \lambda_x, \lambda_y, \lambda_z)/\partial F_i = 0$, and let $3EJ = 1$, we have

$$F_i l_i^3 = \lambda + \lambda_{xi} \bar{x}_i + \lambda_{yi} \bar{y}_i + \lambda_{zi} \bar{z}_i. \tag{17}$$

Substituting the above formula into (16) yields

$$\begin{bmatrix} \sum_{i=1}^{n} l_i^{-3} & \sum_{i=1}^{n} \bar{x}_i l_i^{-3} & \sum_{i=1}^{n} \bar{y}_i l_i^{-3} & \sum_{i=1}^{n} \bar{z}_i l_i^{-3} \\ \sum_{i=1}^{n} x_{Gi} l_i^{-3} & \sum_{i=1}^{n} x_{Gi} \bar{x}_i l_i^{-3} & \sum_{i=1}^{n} x_{Gi} \bar{y}_i l_i^{-3} & \sum_{i=1}^{n} x_{Gi} \bar{z}_i l_i^{-3} \\ \sum_{i=1}^{n} y_{Gi} l_i^{-3} & \sum_{i=1}^{n} y_{Gi} \bar{x}_i l_i^{-3} & \sum_{i=1}^{n} y_{Gi} \bar{y}_i l_i^{-3} & \sum_{i=1}^{n} y_{Gi} \bar{z}_i l_i^{-3} \\ \sum_{i=1}^{n} z_{Gi} l_i^{-3} & \sum_{i=1}^{n} z_{Gi} \bar{x}_i l_i^{-3} & \sum_{i=1}^{n} z_{Gi} \bar{y}_i l_i^{-3} & \sum_{i=1}^{n} z_{Gi} \bar{z}_i l_i^{-3} \end{bmatrix} \begin{Bmatrix} \lambda \\ \lambda_x \\ \lambda_y \\ \lambda_z \end{Bmatrix} = \begin{Bmatrix} F_K \\ F_K x_K \\ F_K y_K \\ F_K z_K \end{Bmatrix}.$$

After solving the above linear equation to obtain the value of the Lagrange multiplier $\lambda, \lambda_x, \lambda_y, \lambda_z$ and then bringing it into the (17), the forces $F_i$ on the structure nodes are assigned.

### 3.4. Inverse distance weighted method.

The main purpose of IDW is to allocate more force on the structure nodes close to the fluid node $K$. The weight of force allocated on each structure node is decided by the inverse of Euclidean distance $l_i$. Therefore the force allocated on each structure

node can be easily calculated by

$$F_i = \frac{1/(l_i)^\alpha}{\sum_{i=1}^{n} 1/(l_i)^\alpha} F_K,$$

where $\alpha$ is a parameter adjusting the weights. We use $\alpha = 1$ in the tests below. It is clear that the force is preserved, while the conservations of moment and virtual work are not maintained in this method.

Among the four conventional force transportation methods, the conservations of force,moment and virtual work are maintained by the VWC. However, it usually causes an unreasonable local force distribution. The local methods, AWSF, PMSE, and IDW,produce the relatively reasonable force distributions, compared with the VWC, but the physical conservations are destroyed. Specifically, the virtual works are not maintained by all three methods, while the moments are not preserved by the AWSF and IDW. Moreover, in the AWSF some structure nodes may get no force, and in the PMSE, local force deviations may appear in areas with high curvatures or irregular distributions of structure nodes.

## 4. A corrected nearest neighbor transportation method

In this section we propose a corrected nearest neighbor transportation method (CNNT) of aerodynamic forces for the fluid-structure coupling analysis. The force transportation process is divided into two phases. First, the aerodynamic forces are allocated to the structural nodes initially using the above-mentioned methods or their combinations, e.g., AWSF, IDW, where the IDW is relatively preferable because of its excellent local performance and easy implementation. The initially allocated forces are denoted by $\mathbf{F}_G^0 = \{F_{Gi}^0\}_{i=1}^{n_G}$. Second, the initially allocated structural forces $\mathbf{F}_G^0$ are corrected by solving an optimization problem with the physical conservations as its optimization target.

According to this idea, a natural optimization problem to correct is proposed by

$$\begin{aligned} &\min_{F_G} \frac{1}{2}(\mathbf{F}_G^T\mathbf{u}_G - \mathbf{F}_K^T\mathbf{u}_K)^2 \\ &\text{s.t.} \begin{cases} \mathbf{Q}_G\mathbf{F}_G = \mathbf{M}_K \\ (1-\varepsilon)\mathbf{F}_G^0 \le \mathbf{F}_G \le (1+\varepsilon)\mathbf{F}_G^0 \end{cases}, \end{aligned} \tag{18}$$

where the structure forces $\mathbf{F}_G$ are the optimization variables, $\mathbf{F}_K$ are the fluid forces, and $\mathbf{u}_G, \mathbf{u}_K$ are structure and fluid displacements, respectively. The first equation in the constraints represents the conservation of forces and moments, in which $\mathbf{M}_K$ are the total forces and moments of fluid, and $\mathbf{Q}_G$ is a coefficient matrix to calculate the total forces and moments of structure, which is defined by

$$\mathbf{Q}_G = \begin{bmatrix} \mathbf{Q}_G^1 & \mathbf{Q}_G^2 & \cdots & \mathbf{Q}_G^{n_G} \end{bmatrix}, \mathbf{Q}_G^i = \begin{bmatrix} 1 & 0 & 0 \\ 0 & 1 & 0 \\ 0 & 0 & 1 \\ 0 & -z_{Gi} & y_{Gi} \\ z_{Gi} & 0 & -x_{Gi} \\ -y_{Gi} & x_{Gi} & 0 \end{bmatrix}. \tag{19}$$

The second equation in the constraints of (18) ensures that the force directions are the same as those of initial forces $\mathbf{F}_G^0$, and the force magnitudes vary in small ranges of $\mathbf{F}_G^0$, characterized by a small parameter $\varepsilon$.

As the minimum of virtual work is an objective function, and the force and moment conservations act as constraints, the physical meaning of optimization

problem (18) is quite clear. However, it is extremely difficult to solve since the constraints in (18) involve both equalities and inequalities. To overcome this, we modify the optimization problem (18) to

$$\begin{aligned} &\min_{F_G} \frac{1}{2}(\mathbf{Q}_G\mathbf{F}_G - \mathbf{M}_K)^T(\mathbf{Q}_G\mathbf{F}_G - \mathbf{M}_K) + \frac{1}{2}(\mathbf{F}_G^T\mathbf{u}_G - \mathbf{F}_K^T\mathbf{u}_K)^2 \\ &\text{s.t.}(1-\varepsilon)\mathbf{F}_G^0 \le \mathbf{F}_G \le (1+\varepsilon)\mathbf{F}_G^0. \end{aligned} \tag{20}$$

The idea (20) is to treat the force and moment conservations as a part of the objective instead of the constraints. The scheme (20) only contains the constraints of inequalities, and can be solved efficiently by a barrier interior point method (see [25] ), for example.

We next address the virtual works in the objective of (20). On the one hand, the structure displacements $\mathbf{u}_G$ are determined by the structural forces $\mathbf{F}_G$ as follows:

$$\mathbf{u}_G = \mathbf{A}^{-1}\mathbf{F}_G, \tag{21}$$

where $\mathbf{A}$ is the structure stiffness matrix. On the other hand, let $\tilde{\mathbf{F}}_G$ be the structure forces calculated from $\mathbf{F}_K$ using the VWC method (11), then based on the property (10) of virtual work conservation of VWC, we have

$$\mathbf{F}_K^T\mathbf{u}_K = \tilde{\mathbf{F}}_G^T\mathbf{u}_G = \tilde{\mathbf{F}}_G^T\mathbf{A}^{-1}\mathbf{F}_G. \tag{22}$$

Substituting (21) and (22) into(20), the optimization problem (20)is rewritten as

$$\begin{aligned} &\min_{F_G} \frac{1}{2}(\mathbf{Q}_G\mathbf{F}_G - \mathbf{M}_K)^T(\mathbf{Q}_G\mathbf{F}_G - \mathbf{M}_K) + \frac{1}{2}(\mathbf{F}_G^T\mathbf{A}^{-1}\mathbf{F}_G - \tilde{\mathbf{F}}_G^T\mathbf{A}^{-1}\mathbf{F}_G)^2 \\ &\text{s.t.}(1-\varepsilon)\mathbf{F}_G^0 \le \mathbf{F}_G \le (1+\varepsilon)\mathbf{F}_G^0, \end{aligned} \tag{23}$$

which is equivalent to

$$\begin{aligned} &\min_{F_G} D(\mathbf{F}_G) := \frac{1}{2}\mathbf{F}_G^T\mathbf{H}\mathbf{F}_G + \mathrm{f}^{\mathrm{T}}\mathbf{F}_{\mathrm{G}} + \frac{1}{2}(\mathbf{F}_{\mathrm{G}}^{\mathrm{T}}\mathbf{A}^{-1}\mathbf{F}_{\mathrm{G}} - \tilde{\mathbf{F}}_{\mathrm{G}}^{\mathrm{T}}\mathbf{A}^{-1}\mathbf{F}_{\mathrm{G}})^2 \\ &\text{s.t.}(1-\varepsilon)\mathbf{F}_G^0 \le \mathbf{F}_G \le (1+\varepsilon)\mathbf{F}_G^0, \end{aligned} \tag{24}$$

in which

$$\mathbf{H} = \mathbf{Q}_G^T\mathbf{Q}_G \quad \text{and} \quad \mathrm{f}^{\mathrm{T}} = \mathbf{M}_{\mathrm{K}}^{\mathrm{T}}\mathbf{Q}_{\mathrm{G}}. \tag{25}$$

We present a barrier interior point method to solve (24). For simplicity, we denote

$$\mathbf{UP} = (1+\varepsilon)\mathbf{F}_G^0 \quad \text{and} \quad \mathbf{DOWN} = (1-\varepsilon)\mathbf{F}_G^0, \tag{26}$$

and a standard log-barrier function (see [25] ) is defined as

$$B(\mathbf{F}_G, \mu) = D(\mathbf{F}_G) - \mu\left[\sum_{i=1}^{n_G}\log(F_{Gi} - \mathbf{DOWN}_i) + \sum_{i=1}^{n_G}\log(\mathbf{UP}_i - F_{Gi})\right], \tag{27}$$

where $\mu > 0$ is barrier factor. The algorithm for solving the optimization problem (24) is described as the following:

Step 1. Give an initial interior point $\mathbf{F}_G^0$, with $\mu_1, \delta_1 > 0, \delta_2 > 0, k := 1$.

Step 2. Taking $\mathbf{F}_G^{k-1}$ as an initial point, solve the nonlinear minimization problem $\mathbf{F}_G^k(\mu_k) = \mathrm{argmin}_{\mathbf{F}_G} B(\mathbf{F}_G, \mu_k)$ and the iteration stops when $\|\nabla B(\mathbf{F}_G^k(\mu_k), \mu_k)\| \le \delta_1$.

Step 3. When $\mu\left|\sum_{i=1}^{n_G}\log(F_{Gi}^k(\mu_k) - \mathbf{DOWN}_i) + \sum_{i=1}^{n_G}\log(\mathbf{UP}_i - F_{Gi}^k(\mu_k))\right| \le \delta_2$, the iteration stops; otherwise, chose $\mu_{k+1} < \mu_k$ and $\mathbf{F}_G^k = \mathbf{F}_G^k(\mu_k)$, go to step 2.

Based on this barrier interior point method, the optimization problem (24) can be solved efficiently, and all the conservations of forces, moments, and virtual works are achieved, as shown in the numerical experiments.

We mention that the choice of sequence $\mu_k$ will affects the barrier interior point method. In our computations, we use

$$\mu_1 = D(\mathbf{F}_G)/\left(1/\sum_{i=1}^{n_G}(F_{Gi}^k(\mu_k) - \mathbf{DOWN}_i) + 1/\sum_{i=1}^{n_G}(\mathbf{UP}_i - F_{Gi}^k(\mu_k))\right),$$

and $\mu_{k+1} = \alpha\mu_k, 0 < \alpha < 1.$

The parameters $\alpha$ and $\delta_2$ are problem-dependent. For instance, a large $\alpha$ may slow the convergence rate, while a small $\alpha$ may make the iteration stop too early to find a good optimal solution.

The calculation process of the CNNT in a bigger flow chart of the general fluid-structure coupling analysis process is illustrated in FIGURE 5, and we also describe it below,

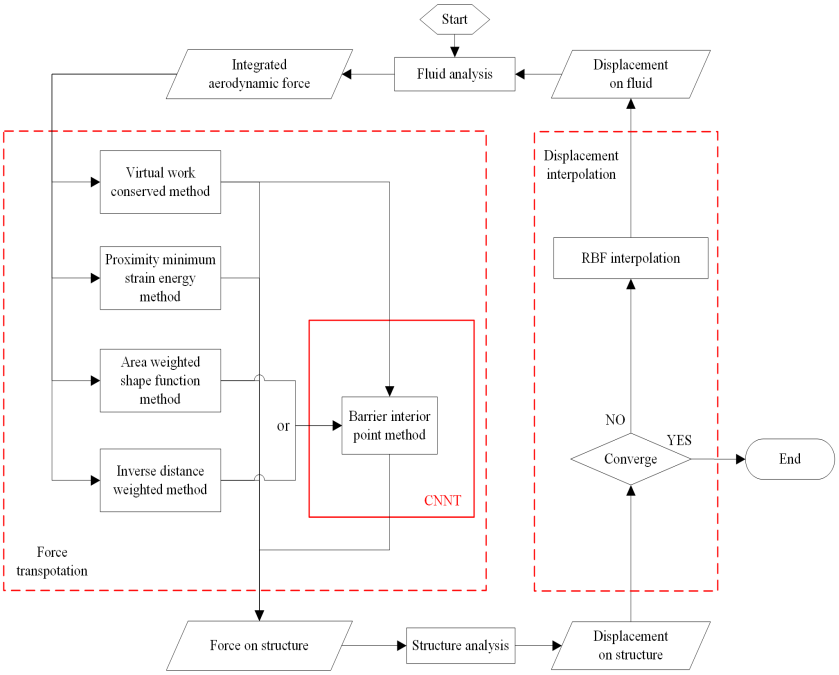


FIGURE 5. CNNT method within the fluid-structure coupling flow chart.

1) Obtain the pressure distribution from fluid analysis and integrate into a concentrated force at the center point of the fluid element.

2) Transform the fluid force to be the structure force using the proposed CNNT.

3) After the displacement of the structural nodes is obtained from structural analysis, the RBF interpolation based on TPS (in Section 2) is used to accurately interpolate the displacement from the structure node to the fluid element grid.

4) Calculate the new pressure distribution according to the deformation.

5) Repeat step 4), 1), 2), 3) until the iteration converges to complete the fluid-structure coupling analysis.

**Remark 4.1**.The optimization problem (24) keeps the global conservations of physical quantities. The idea can be extended to the conservations on various regions of an aircraft similarly, for instance, on the nth region, by adding the following functions into the objective of (24):

$$D_n(\mathbf{F}_G) := \frac{1}{2}\mathbf{F}_G^T\mathbf{C}_n^T\mathbf{H}\mathbf{C}_n\mathbf{F}_G + \mathrm{f}^{\mathrm{T}}\mathbf{C}_{\mathrm{n}}\mathbf{F}_{\mathrm{G}} + \frac{1}{2}(\mathbf{F}_{\mathrm{G}}^{\mathrm{T}}\mathbf{C}_{\mathrm{n}}^{\mathrm{T}}\mathbf{A}^{-1}\mathbf{F}_{\mathrm{G}} - \tilde{\mathbf{F}}_{\mathrm{G}}^{\mathrm{T}}\mathbf{C}_{\mathrm{n}}^{\mathrm{T}}\mathbf{A}^{-1}\mathbf{F}_{\mathrm{G}})^2, \tag{28}$$

where $\mathbf{C}_n$ is the selection matrix related to the $n$th region. Using this way, both the global and region conservations can be dealt with.

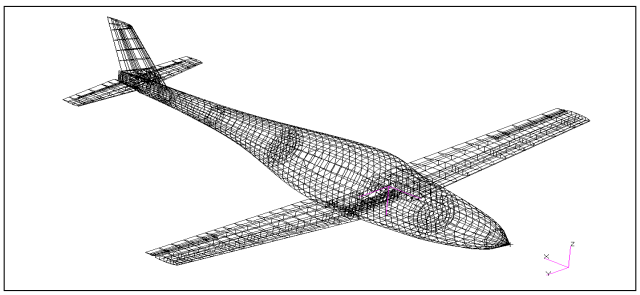

FIGURE 6. Structure model in finite element method.

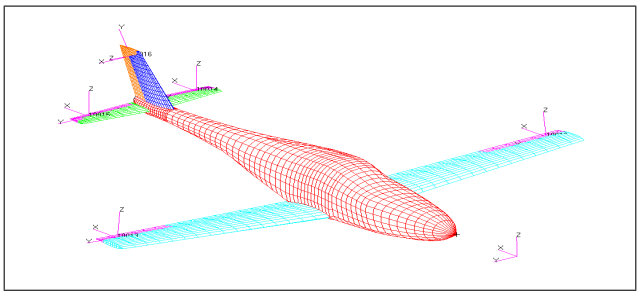

FIGURE 7. Fluid model in high-order panel method.

## 5. Numerical experiments

An example of sport plane is used to make comparison of different aerodynamic force transportation methods. The structure model comes from the numerical example of MSC.NASTRAN named freedlm.dat, which is shown in FIGURE 6. This finite structure model is constructed by shell and beam element, and solved by finite elements methods.

The fluid model is restored from the structure, which is shown in FIGURE 7, and solved by high-order panel methods [26]. In geometry, the wing aspect ratio is 10 and dihedral angle is 5 degree, with 8.3614m$^2$ in area, 0.9144m in chord and 9.144m in span. About three thousands panel elements are meshed to perform fluid analysis in high-order panel method. The pressure result is given in the form of constant in a panel.

A fluid-structure coupling case of 0.4 Mach number in speed, 25063.55Pa in dynamic pressure and 4 degree in attack angle is executed. In the CNNT, both of global conservation and upper wing region conservation are considered to construct the object function. And $\varepsilon = 10\%$ is selected in (24) to limit the range of force on

TABLE 1. Total integrated load in different methods.

| | Fx | Fy | Fz | Mx | My | Mz |
|---|---|---|---|---|---|---|
| Fk | -480.192 | -388.592 | 5568.437 | 384242.940 | 27266.236 | 36803.670 |
| Fg_VWC | -480.192 | -388.592 | 5568.437 | 384242.940 | 27266.236 | 36803.667 |
| Error_V | 0.00% | 0.00% | 0.00% | 0.00% | 0.00% | 0.00% |
| Fg_PMSE | -480.192 | -388.592 | 5568.437 | 384242.941 | 27266.236 | 36803.667 |
| Error_P | 0.00% | 0.00% | 0.00% | 0.00% | 0.00% | 0.00% |
| Fg_AWSF | -480.192 | -388.592 | 5568.437 | 382400.284 | 27270.035 | 36599.718 |
| Error_A | 0.00% | 0.00% | 0.00% | -0.48% | 0.01% | -0.55% |
| Fg_IDW | -480.192 | -388.592 | 5568.437 | 386855.984 | 28156.183 | 36954.730 |
| Error_I | 0.00% | 0.00% | 0.00% | 0.68% | 3.26% | 0.41% |
| Fg_A-CT | -480.192 | -388.592 | 5568.437 | 384242.939 | 27266.236 | 36803.670 |
| Error_A-CT | 0.00% | 0.00% | 0.00% | 0.00% | 0.00% | 0.00% |
| Fg_I-CT | -480.192 | -388.597 | 5568.431 | 384243.123 | 27265.558 | 36804.286 |
| Error_I-CT | 0.00% | 0.00% | 0.00% | 0.00% | 0.00% | 0.00% |

structure. As for the force transportation method, 16 nearest structure nodes to a fluid point are chosen in PMSE and IDW.

As the wing region occupies most percentage of physical parameters of the global airplane in this case, only the results of the right side upper wing is selected to make a comparison in different force transportation methods. The results of whole airplane are similar, and we do not present them here. The fluid mesh of the right side upper wing is shown in FIGURE 8 with 204 elements (center point of which is the fluid point), with 191 corresponding structure nodes.The total integrated results and local distribution results of the right-side upper wing region are listed below.

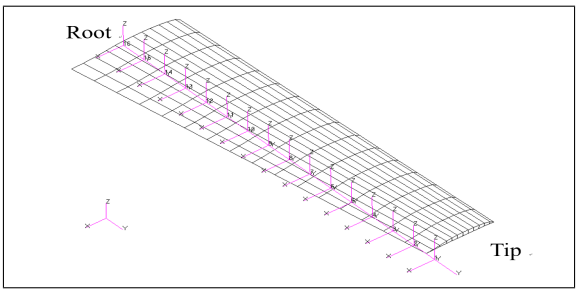


FIGURE 8. Fluid mesh and integration coordinates of the right side upper wing.

### 5.1. Total integrated results.

In the process of force transportation, four conventional methods, VWC (suffixed by 'V'), PMSE (suffixed by 'P'), AWSF (suffixed by 'A') and IDW (suffixed by 'I') are first implied. Then CNNT results based on AWSF and IDW are respectively applied and suffixed by '-CT'. The original force on fluid is expressed by 'Fk', while force on structure is represented by 'Fg'. In this way, results of total force (Fx, Fy, Fz), moment (Mx, My, Mz) in three directions and total virtual work (Wk for fluid, Wg for structure) are integrated at the coordinate in the root of the right-side upper wing in FIGURE 8 and listed below.

TABLE 2. Total virtual work in different methods.

| | VWC | PMSE | AWSF | IDW | AWSF-CT | IDW-CT |
|---|---|---|---|---|---|---|
| Wk | 21841.130 | 21856.708 | 21723.491 | 21984.785 | 21914.772 | 22090.281 |
| Wg | 21841.130 | 21872.514 | 21604.742 | 22093.595 | 21914.765 | 22090.276 |
| Error | 0.00% | 0.07% | -0.55% | 0.49% | 0.00% | 0.00% |

Its obvious that force can be all preserved in four conventional transportation method in TABLE 1, but only VWC and PMSE can maintain the conservation of moment. AWSF cause small errors in moments in three dimension although it is moment conservative in two dimension. The IDW causes larger error in moments as no moment conservation law is included in the algorithm. Nevertheless, the moments of CNNT are perfectly preserved as shown in the row of Fg_A-CT and Fg_I-CT.

As displacement is decided by force, different fluid virtual works of Wk and structure virtual work Wg would be obtained in different methods, as shown in TABLE 2.

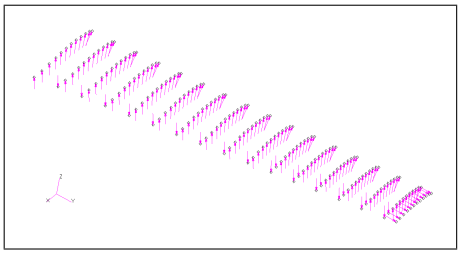

(a) Fk

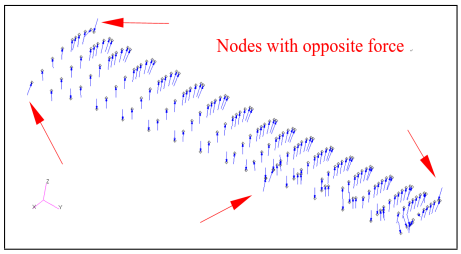


(b) VWC

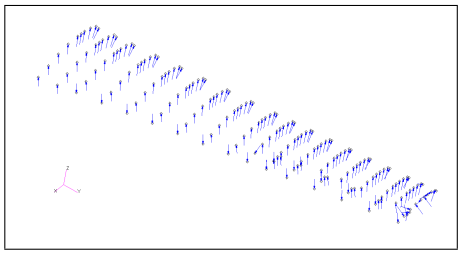

(c) PMSE

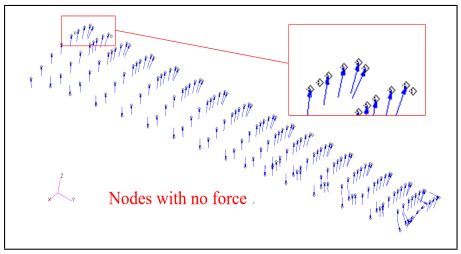


(d) AWSF

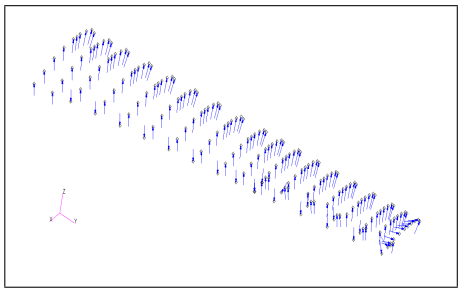

(e) IDW

FIGURE 9. Fluid mesh and integration coordinates of the right side upper wing.

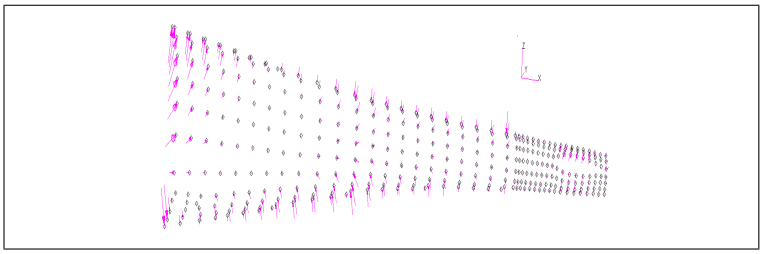

(a) Fk

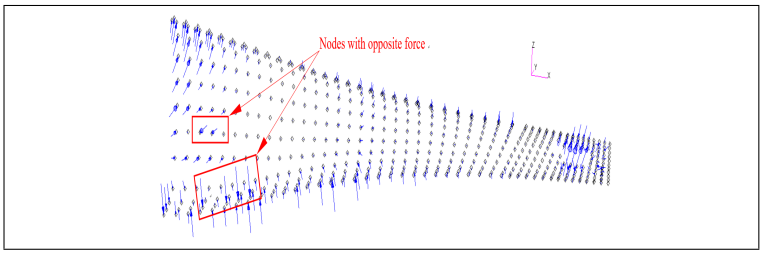


(b) PMSE

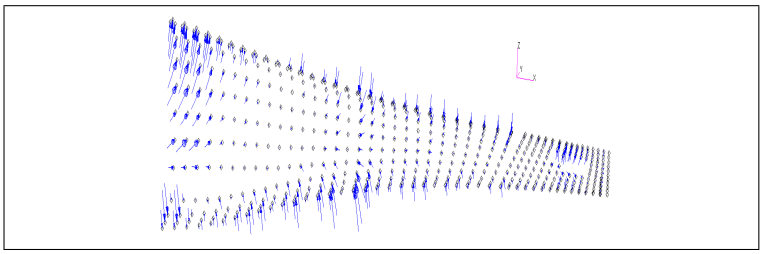

(c) IDW

FIGURE 10. Force magnitude of rear fuselage.

From the results of TABLE 2, it can be first concluded that VWC perfectly maintains the conservation of virtual works, as predicted by the theory of VWC. The PMSE, AWSF and IDW all lead to relatively larger error in virtual works. Based on the CNNT, the virtual work errors of AWSF-CT and IDW-CT decrease to almost zero.Therefore, the CNNT method can successfully achieve the global conservations based on an initial force distribution of local force transportation methods that is not originally conservative.

We mention that the errors caused by conventional force transportation methods seem to not large. But with hundreds time of iterations in loose fluid-structure coupling analysis, the errors may accumulate into very large ones.

### 5.2. Local distribution results.

As the local performance is also an important aspect in force transportation, force direction, force distribution and integrated result along the wing are compared for different methods.

#### 5.2.1. Force direction.

The CNNT does not change the direction of initial value, so the force direction is compared only in conventional transportation methods below in FIGURE 9.

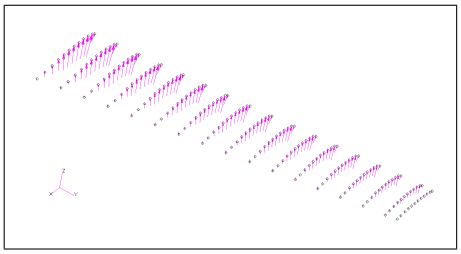

(a) Fk

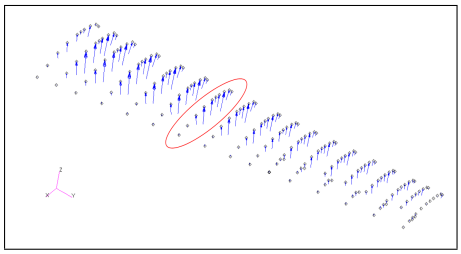

(b) VWC

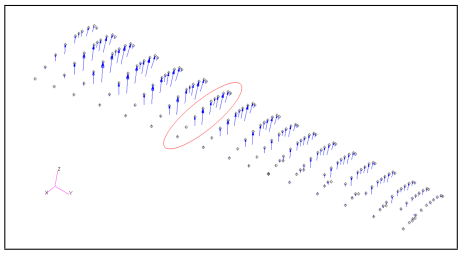

(c) PMSE

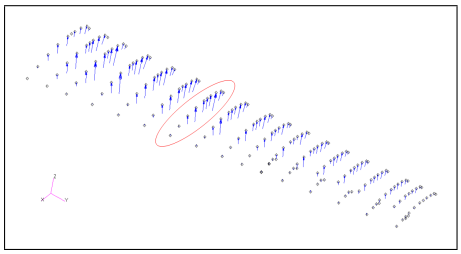

(d) AWSF

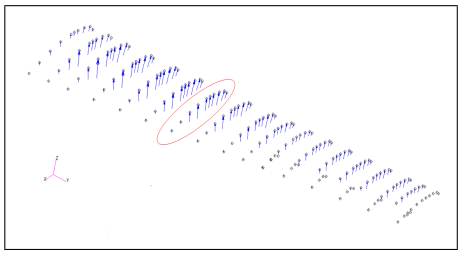

(e) IDW

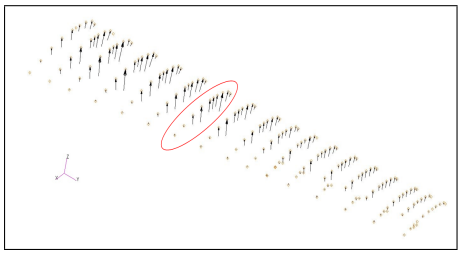

(f) AWSF-CT

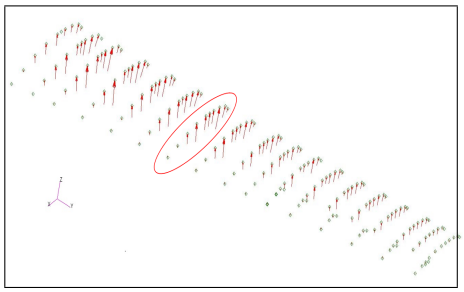

(g) IDW-CT

FIGURE 11. Force magnitude in different methods.

Most force directions in the initial aerodynamic forces Fk are upward, except several downward forces at the trailing edge and lateral ones at the tip of the wing. We see from FIGURE 9 that in the VWC, nodes with unreasonable opposite force appear. In the AWSF, there are nodes allocated with no force, as only three nodes are chosen for each fluid node. But in the IDW, almost all the force directions are kept (force in the tip is ignored for its little magnitude) and no missed nodes exist. The PMSE seems to have the same good local performance, but behaves

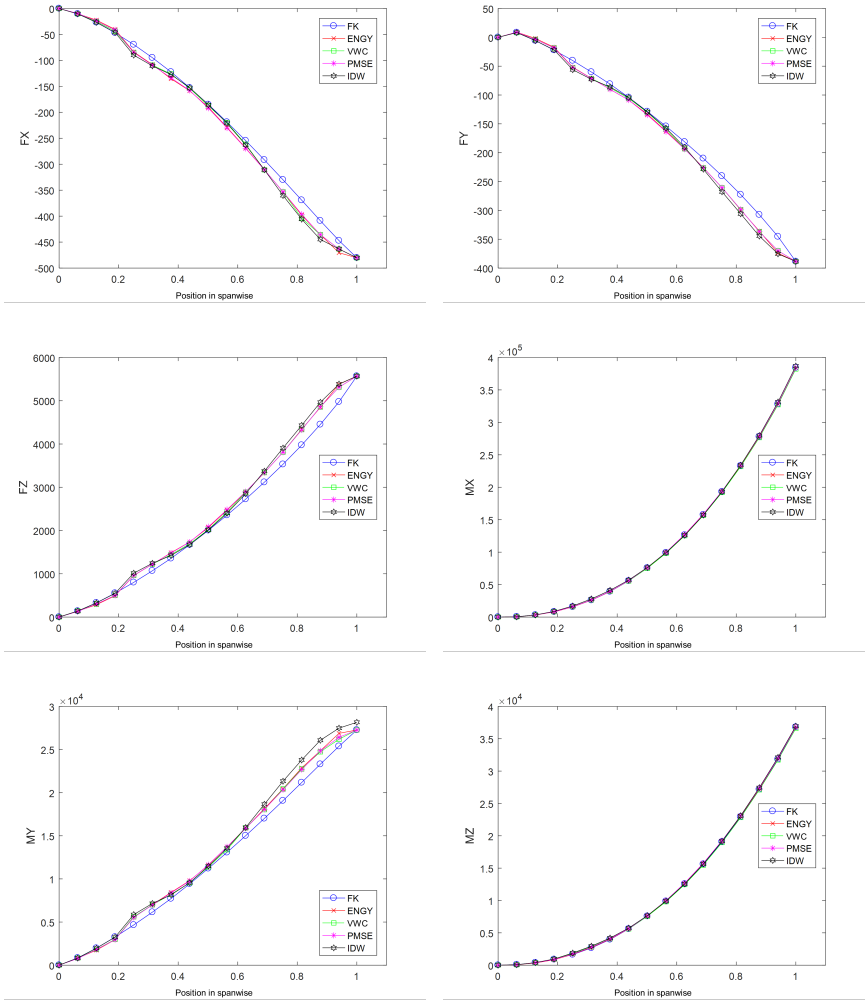


FIGURE 12. Force and moment in four conventional force transportation methods.

badly on large curvature region like the rear fuselage, as shown within the red box in FIGURE 10.

### 5.2.2. Force distribution.

The force magnitude is a representation of the force distribution. How similar structure force distribution is to the original force distribution of fluid is another criterion to judge the local force performance. Force magnitude of all the methods used in this paper are compared in FIGURE 11.

In FIGURE 11, the VWC and PMSE demonstrate significant difference with Fk as circled in red ellipse. AWSF is better than VWC and PMSE. IDW almost maintain the distribution of Fk. As only 10% float is allowed around the initial distribution, the changes of distribution are not obvious in the CNNT. Therefore, CNNT based on IDW obtain better force distribution than the one based on AWSF.

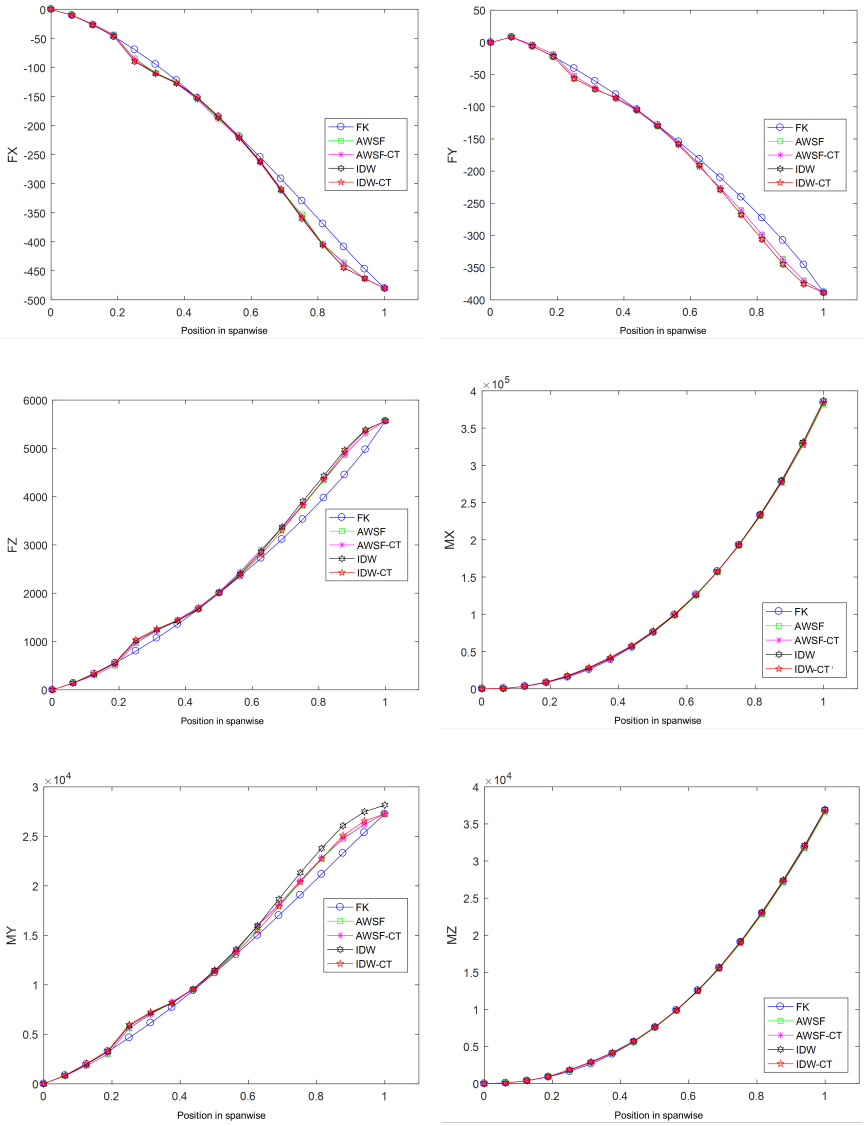


FIGURE 13. Force and moment in the CNNT based on AWSF and IDW.

### 5.3. Integral force and moment.

The integrated force and moment diagram of four conventional force transportation methods are illustrated in FIGURE 12, by integrating the force in FIGURE 11 from tip (0.0 in spanwise) to root (1.0 in spanwise) with the coordinate listed in FIGURE 8.The integrated force and moment results of CNNT is illustrated in FIGURE 13.

By comparing the curves in FIGURE 12, it can be concluded that the magnitude of integrated force with any transportation methods is always larger than the original result of Fk. This may be caused by the position of integrating section. On the other hand, the IDW shows more deviation than the other three conventional transportation methods. In FIGURE 13, based on the CNNT, the deviation of

IDW decreases as shown in IDW-CT curve. Although IDW-CT curve is as close to Fk as AWSF-CT, it is still obviously different from AWSF-CT.

## 6. Conclusions

In this paper we presented a new aerodynamic force transportation method, the corrected nearest neighbor transportation method (CNNT), to guarantee the conservations of virtual work, forces and moments, and the consistency of local force distributions in a fluid-structure coupling problem. The CNNT treats the aerodynamic force transportation in two phases. First, the aerodynamic forces are allocated initially to the structural nodes using the conventional approaches, such as AWSF, IDW. Then the initially allocated forces are corrected based on an optimization problem, which can be solved by a barrier interior point method efficiently. The proposed method is tested using a sport airplane, and numerical experiments show its effectiveness. The comparisons with the conventional methods, e.g., VWC, PMSF, AWSF, and IDW were made to demonstrate that the CNNT is the only method to preserve the conservations of physical quantities required and reasonable distributions of forces indeed. Additionally, the CNNT is very flexible and can be generalized to situations that the conservations of laws are maintained on both the whole aircraft and its various sub-regions.

The CNNT incorporates solving the barrier interior point method. However, the increase in computational cost is slight with respect to in the whole fluid-structure coupling computation. Therefore, the CNNT can be applied to large airplane analysis without special treatment. Besides, as aerodynamic force transformation is only a part of loose coupling, and loose coupling is a generally used method both in static and dynamical aeroelastic problems, CNNT can be directly applied in dynamical aeroelastic problems. An extension of CNNT to dynamical aeroelasticity analysis will be studied in a forthcoming research.

## Acknowledgments

This research was partially supported by the Natural Science Foundation of China under grants 91730305, 11971499, 11701189, and Guangdong Provincial Natural Science Foundation of China under grant 2015A030306016.

## References

[1] A. de Boer, A.H. van Zuijlen, and H. Bijl, Review of coupling methods for non-matching meshes, Computer Methods in Applied Mechanics and Engineering, 196: 1515-1525, 2007.
[2] W. G. An, S. Y. Liang, and D. Y. Chen, Local Dynamic Data Exchange in Fluid Structure Interaction Analysis, Acta aeronautica et astronautica Sinica, Vol.3 4 No.3., 2013.
[3] B. Su, R. J. Qian, and X. F. Yuan, Advances in research on theory and method of data exchange on coupling interface for FSI analysis, Spatial structures, Vol.16 No.1, 2010.
[4] E. K. J. Bath, H. Zhang, and J. Shan, Finite element analysis of fluid flows fully coupled with structural interactions, Computers & Structures, 72: 1-16, 1999.
[5] W. Dettmer and D. Peric, A computational framework for fluid-rigid body interaction: finite element formulation and applications, Computer Methods in Applied Methanics and Engineering, 195: 1633-1666, 2006.
[6] K. Stein, R. Benney, V. Kalro, et al, Parachute fluid-structure interactions: 3-D computation, Computer Methods in Applied Mechanics and Engineering, 190: 373-386, 2000.
[7] G. S. L. Goura, K. J. Badcock, M. A. Woodgate, et al, A data exchange method for fluid-structure interaction problems, The Aeronautical Journal, (105): 215-221, 2001.
[8] L. H. Robert, T. Robert, and N. Desmarais, Interpolation using surface splines, Journal of Aircraft, 9: 189-191, 1972.
[9] K. Appa, Finite-surface spline, Journal of Aircraft, 26: 495-496, 1989.
[10] J. Duchon, Splines minimizing rotation-invariant semi-norms in Sobolev spaces, Constructive theory of functions of several variables, Springer Berlin / Heidelberg, 1976.

[11] R. L. Hardy, Multiquadric equations of topography and other irregular surfaces, Journal of Geophysics Research, 76: 1905-1915, 1971.
[12] D. Shepard, A two dimensional interpolation function for regularly spaced data, Proceedings of 23d National Conference of the Association for Computing Machinery, Princeton, NJ, ACM, :517-524, 1968.
[13] Z.M. Wu, Radial Basis Function Scattered Data Interpolation and the Meshless Method of Numerical Solution of PDEs, Journal of engineering mathematics, Vol.19 No .2, 2002.
[14] M. D. Buhmann, Radial basis functions: theory and implementations, Cambridge University Press, 2004.
[15] Y. Sun, D. H. Meng, Y. T. Wang, and X.G. Deng, Dynamic grid deformation method based on radial basis function and hybrid background grid, Acta Aeronautica et Astronautica Sinic, Vol.37 No.5, 2016.
[16] M. S. Mohamed, R. P. Koomullil, and R. M. David, Finite Volume Based Fluid-Structure Interaction Solver, AIAA SciTech Forum, Grapevine, Texas, 2017.
[17] K. E. Jacobson, J. F. Kiviaho, M. J. Smith, and G. J. Kennedy, An Aeroelastic Coupling Framework for Time-accurate Aeroelastic Analysis and Optimization, AIAA SciTech Forum, Kissimmee, Florida, 2018.
[18] A. Murray, B. Thornber, M. Flaig, and G. Vio, Highly Parallel, Multi-stage Mesh Motion using Radial Basis Functions for Fluid-Structure Interaction, AIAA SciTech Forum, San Diego, California, 2019.
[19] M. J. Smith, C. E. S. Cesnik, and D. H. Hodges, Evaluation of some data transfer algorithms for noncontiguous meshes, J. Aerospace Engineering, 13: 52-58, 2000.
[20] M. J. Smith, D. H. Hodges, and C. E. S. Cesnik, Evaluation of computational algorithms suitable for fluid-structure interactions, J. Aircraft, 37: 282-294, 2000.
[21] MSC/Nastran, Aeroelasticity, 2005.
[22] M. K. Bhardwaj, R. K. Kapania, and R. Eric, A CFD/CSD interaction methodology for aircraft wings, AIAA 98-4783, 1998.
[23] T. Q. Ye and T. X. Zhou, Aviation structural finite element analysis guide, Beijing: Aviation Industry Press, P177, 1996.
[24] G. Y. Zong, H. H. Chen, K. C. Chang, T. Wu, and T. Cebeci, A general method for calculating aeros-structure interaction on aircraft configurations, AIAA Meeting Papers on Disc, pp. 14-24, 1996.
[25] L. Gao, Numerical optimization method, Peking University Press, pp.194-195, 2014.
[26] Y.Z. Liu, Z.Q. Wan, and Chao Yang, A High Efficiency Aeroelastic Analysis Method based on Rigid External Aerodynamic Force and Elastic Correction by High-Order Panel Method, AIAA SciTech Forum, Grapevine, Texas, 2017.

Yunzhen Liu and Zhiqiang Wan, School of Aeronautic Science and Engineering, Beihang University, Beijing, 100191, PR China

*E-mail*: liuyunzhen@buaa.edu.cn and wzq@buaa.edu.cn

Qia Li and Qinghui Zhang, Guangdong Province Key Laboratory of Computational Science and School of Data and Computer Science, Sun Yat-Sen University, Guangzhou, 510006, PR China

*E-mail*: liqia@mail.sysu.edu.cn and zhangqh6@mail.sysu.edu.cn